Proximity Binding Assay for PROTAC Ternary Complex Analysis

Ponzo, Irene; Soldà, Alice; Crowe, Charlotte; Dahl, Göran; Jahodová, Tereza; Heerwig, Andreas

Published in:
ACS Sensors

DOI:
10.1021/acssensors.5c04944

Publication date:
2026

ACS SENSORS

pubs.acs.org/acssensors
Article

Proximity Binding Assay for PROTAC Ternary Complex Analysis

Irene Ponzo,[†] Alice Soldà,[†] Charlotte Crowe, Göran Dahl, Tereza Jahodová, Andreas Heerwig, Stefan Geschwindner,* Alessio Ciulli,* and Ulrich Rant*

Cite This: https://doi.org/10.1021/acssensors.5c04944

ABSTRACT: The engineered formation of ternary complexes, in which two proteins are bridged by small molecules such as PROTACs or molecular glues, is a prerequisite for the targeted enzymatic degradation of pathogenic proteins; however, the combined analysis of these ternary interactions during the drug discovery process remains challenging. Here, we introduce a proximity binding assay for the simultaneous measurement of binary and ternary interaction kinetics on a biosensor surface. Target proteins and the substrate binding subunit of ubiquitin E3 ligase are tethered to mobile swivel arms of a Y-shaped DNA scaffold. The Y-structure induces spatial proximity between the proteins and presents them to PROTAC analytes flown across the sensor. PROTAC-induced ternary complex formation is measured by fluorescence energy transfer (FRET), while binary interactions are detected by fluorescence quenching. The assay is applied to cereblon (CRBN) and von Hippel-Lindau (VHL) as E3 ligase substrate receptors, a range of compounds including AT1, MZ1, dBETs, and ARV-825 as PROTACs, and the two bromodomains of BRD2, BRD3, BRD4, and BRDT proteins as targets. Automated workflows enable the measurement of 384 real-time sensorgrams in a single run using picomole sample quantities. The insights into proximity-mediated binding kinetics can enable the development of PROTACs and molecular glues with improved properties for targeted protein degradation.

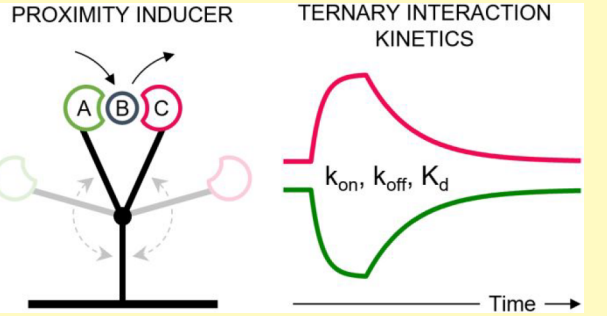

KEYWORDS: *targeted protein degradation, PROTAC, molecular glue, ternary complex, kinetics, affinity, avidity, Y-structure, switchSENSE, CRBN, VHL, BRD, BET*

Initially described in 2001,[1,2] PROTACs (PROteolysis TArgeting Chimeras) have emerged as a powerful therapeutic compounds to selectively degrade proteins via the ubiquitin-proteasome system (UPS). PROTACs are bifunctional small molecules consisting of two protein-binding moieties joined by a linker: one moiety targets a protein of interest (POI), while the other recruits an E3 ubiquitin ligase. By simultaneously engaging both the E3 ligase and the POI, a ternary complex is formed, which enables ubiquitination and subsequent degradation of the POI. Similarly, molecular glues also induce ternary complex formation, albeit via distinct molecular structures and mechanism. PROTACs and molecular glues are promising therapeutic modalities because they enable catalytic and event-driven pharmacology that can extend drug discovery to proteins that are difficult to inhibit by conventional small molecules.[3] Targeted protein degradation has recently been applied successfully also to receptors on cell surfaces using bispecific antibodies (PROTABs).[4,5] Most common PROTACs are recruiters of von Hippel-Lindau (VHL)[6,7] and cereblon (CRBN-DDB1).[8,9] These substrate receptors are components of the Cullin-RING E3 ligase (CRL) complexes $CRL2^{VHL}$ and $CRL4^{CRBN}$. In particular, CRBN was identified as the molecular target of the immunomodulatory imide (IMiDs) drugs, thalidomide and derivatives, that are indicated for multiple myeloma,[10] and many PROTACs in clinical trials recruit CRBN as the E3 ligase. One of the most studied PROTAC targets is BRD4, belonging to the BET family of proteins. BRD4 contains two bromodomains, BD1 and BD2, known to be involved in the transcriptional regulation of gene expression.[11]

The formation of a ternary complex between the target protein, the PROTAC, and the E3 ligase, is key to the PROTAC's mechanism of action and efficient target protein degradation.[6,12−16] Thus, a detailed understanding of how to induce and maintain ternary interactions is essential. In vitro biophysical assays are attractive compared to cellular assays and in vivo methods for their well-defined experimental conditions and ease-of-use. The analysis of binding parameters such as affinity, avidity, and cooperativity can reveal useful details about complex formation and stability, and hence guide drug design.

Received: December 26, 2025
Revised: April 4, 2026
Accepted: April 6, 2026

https://doi.org/10.1021/acssensors.5c04944
ACS Sens. XXXX, XXX, XXX−XXX

The measurement of association and dissociation kinetics can be especially insightful as it addresses two important questions: how quickly does a PROTAC engage its cognate POI and E3 ligase, and how long does it hold the POI and ligase together to enable ubiquitination?

Scheme 1 illustrates that the ternary complex forms and decays via intermediate binary complexes. The population of binary and ternary states adjusts according to a dynamic interplay of associations, transient dissociations, and re-associations, until eventually complete dissociation ensues. The observable kinetics and the dynamic equilibria of these processes are governed by the molecular reaction rate constants of association and dissociation, k_{on} and k_{off}, the dissociation constant $K_d = k_{off}/k_{on}$, as well as the concentrations of free reactants and binary complexes.

To drive a reaction pathway that effectuates maximal protein degradation, suitable PROTACs or molecular glues with ideal association and dissociation kinetics need to be selected from a (potentially large) pool of candidates. For this purpose, ternary binding must be discriminated from binary binding in a straightforward way.[16] Moreover, the development of high-throughput compatible workflows will facilitate the screening of many compounds. To this end, we developed a chip-based biosensor method—the Y-structure *proximity binding assay* (PBA)—for investigating ternary complex formation with a fluorescence readout. The Y-structure immobilizes two proteins in spatial proximity on a sensor surface, with two differently colored fluorophores positioned nearby to probe binding. This approach enables the direct testing of bifunctional analytes with respect to their ability to form ternary complexes. The term *proximity binding assay* (PBA) was chosen by analogy to the established *proximity ligation assay* (PLA), which similarly translates the spatial proximity of two biomolecules into a detectable signal (albeit through DNA ligation and subsequent rolling circle amplification). Here, we demonstrate a screening assay for PROTACs recruiting two different E3 ligase substrate receptors, VHL and CRBN, and different BET proteins as targets.

RESULTS

Y-Shaped Scaffold for Probing Ternary Complex Formation

A Y-shaped DNA nanostructure was developed, which tethers two different proteins—a target protein and the substrate binding subunit of E3 ligase—to a sensor at 1:1 stoichiometry, see Figure 1A. The Y-structure enables the two proteins to swivel freely at the ends of two arms connected at a pivot point and allows them to interact with each other as well as with a third molecule, the bifunctional PROTAC analyte. The arms are each labeled with a red and a green fluorophore, respectively, at their distal ends for the detection of binding kinetics. Real-time fluorescence intensity changes in two spectral channels were measured with a commercially available biosensor instrument previously used to analyze molecular interactions and multivalent binding.[17−22]

Ternary complex formation was monitored by fluorescence resonance energy transfer (FRET, Figure 1B left). Green fluorophores attached to the POI swivel-arm ("green arm") were excited while emission from red fluorophores attached to the E3 ligase swivel-arm ("red arm") was recorded. Formation of the POI−PROTAC−ligase ternary complex brings the two proteins into close proximity, enabling energy transfer from the green donor to the red acceptor and resulting in a measurable FRET signal. This FRET readout directly measures transitions between binary and ternary states, cf. Schemes 1 and 2.

Scheme 1. Simplified Reaction Scheme for Binary and Ternary Complex Formation and Decay between an E3 Ligase (A), a PROTAC (B), and a Protein-of-Interest (C)[a]

[a]See Scheme S1 in the Supplementary Information for more details.

Binary interactions (PROTAC-POI or PROTAC-ligase) were monitored by fluorescence quenching in either the green or the red spectral channel (Figure 1B, right). In this detection mode, the fluorophore probes the local chemical environment within the reach of its linker. Fluorescence is quenched through dynamic or static interactions with nearby regions of the protein or with bound small molecules or proteins (unquenching can occur but is not observed here). Possible mechanisms include collisional quenching, hydrophobic stacking of aromatic moieties, perturbation of the dye conformation, or intersystem crossing to non-fluorescent triplet states.[25] As a result, fluorescence intensity decreases during association and increases during dissociation, reflecting the fraction of bound molecules.

The Y-structure is made up of a stem that branches into two swivel arms. The 96 bp stem connects the Y-structure to the surface via a sequence that is complementary to 48 nt anchor-strands, which are fixed on a chip with two sensor spots in an integrated microfluidic channel (Figure 1C). The chip was used off-the-shelf, featuring different anchor sequences on each spot for the DNA-encoded functionalization with DNA-protein conjugates. The sensor is functionalized with fresh Y-structures by DNA hybridization, and used Y-structures are removed from the sensor by denaturing the stem in a high-pH wash, both steps being performed in the instrument automatically. The swivel arms are 48 bp long and attached to the stem via a flexible hinge region, which enables the arms to rotate by diffusion. The distal ends of the arms may touch or move away from each other, reaching distances up to 40 nm.

Before applying the Y-structure to PROTAC measurements, we used interactants with known binding affinities to characterize induced proximity. To this end, we extended the arms with overhangs of complementary oligodeoxynucleotides from 4 to 15 bp and tested how long (strong) the oligodeoxynucleotides need to become to close the swivel arms by "zipping" them up at their tips. The zipper dissociation constants were characterized in a separate experiment, using the same biosensor, and span more than nine orders of magnitude from *pM* to *mM* K_d-values (Figures 2A and S1B−E). With the obtained affinities, we can plot the open/closed arm configurations versus the zipper K_d in Figure 2A. For short and weak zippers with less than 6 bp and $K_d^{zipper} > 10$ μM, the arms remain always open, while for long and strong zippers with more than 12 bp and $K_d^{zipper} < 1$ nM, the arms are always closed. When using zippers of intermediate lengths (7−11 bp), the arms are partly open and partly closed. This range of affinities with 1 nM$< K_d^{zipper} <$10 μM can be considered the Y-structure's dynamic range, as arm configurations dynamically switch between open and closed states. The midpoint, at which 50% of the arms are closed when averaged over

https://doi.org/10.1021/acssensors.5c04944
ACS Sens. XXXX, XXX, XXX−XXX

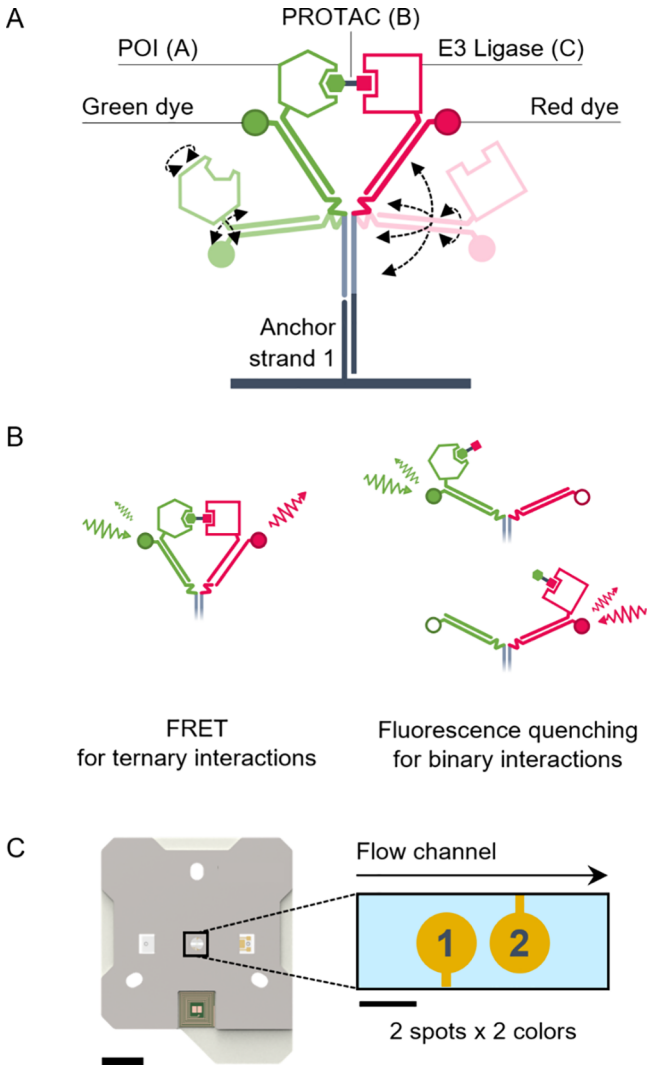

Figure 1. Y-shaped DNA structure for proximity binding assays. (A) Y-structure is made up of a stem and two swivel arms connected by flexible linkers and consists of four DNA strands. The protein-of-interest (POI) and E3 ligase substrate receptor (E3 ligase) are attached to the distal arm ends. Arrows indicate six rotational degrees of freedom for arms' motions relative to the stem and proteins' motions relative to the arms. (B) Detection principles: Green and red fluorophores are attached to the distal ends of the swivel arms to detect ternary binding via fluorescence energy transfer (FRET, left). A FRET signal is generated when the arms are closed. Binary binding is detected via fluorescence quenching that occurs when the local chemical environment around the fluorophore is altered by molecules binding to the adjacent proteins (right). (C) Binding kinetics are measured on two gold spots within the microfluidic channel of a biochip (left scale bar 1 cm; right scale bar 100 μm). Proteins are immobilized on each spot via DNA encoded addressing, utilizing unique anchor strands on the detection spots.

time, is observed for a zipper $K_d^{zipper} = 150$ nM. We may interpret this affinity calibration experiment in terms of an effective concentration: the Y-structure induces a proximity equivalent to an effective concentration of $c_Y = 150$ nM, because if interactants with a $K_d = 150$ nM are attached to the Y-structure's arms, a fraction of 50% is bound. However, we note that the term effective concentration used here is not the same as a solution concentration of molecules diffusing freely in three dimensions, because interactants on a Y-structure are constrained by their attachment to the arms, and the arms' swivel motions.

Scheme 2. Ternary Complex Formation and Decay as Monitored with the Y-Structure FRET Proximity Binding Assay (PBA) and Commonly by SPR[a]

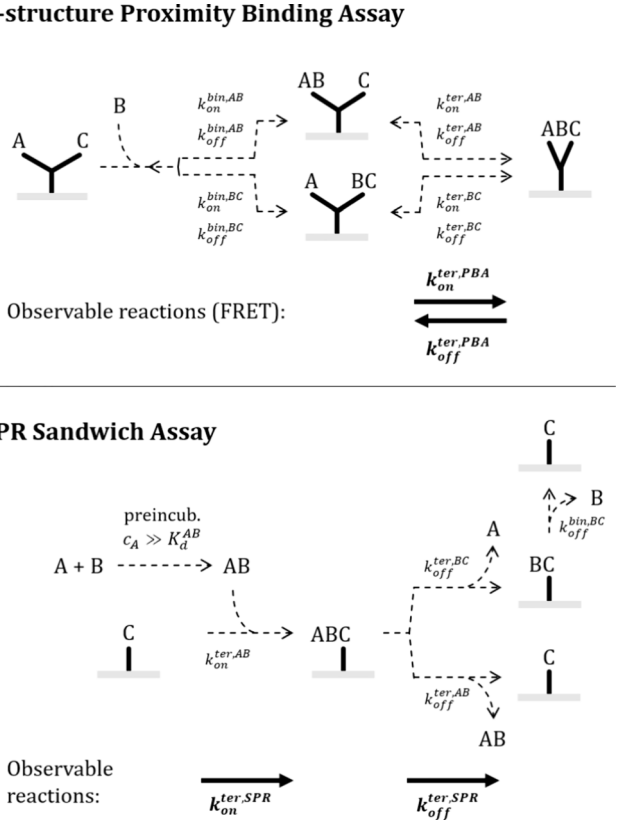

[a]A is the target, B is the PROTAC, and C is the E3 ligase. Bold arrows indicate reactions involving ternary complex formation or decay, which are observable by PBA and SPR, respectively, while dashed lines indicate non-observable reactions.

To further investigate the flexibility of the Y-structure—particularly the constraints on the movement of its arms—we performed molecular dynamics simulations using the coarse-grained oxDNA2 model,[23] attaching the stem at one end to a surface. Snapshots of the molecular configurations reveal that the single-stranded hinge region is highly flexible, allowing the arms to undergo swivel-like motions (Figures 2B and S1F). The 16 nm arms exhibit minimal bending, consistent with their length being significantly shorter than the mechanical persistence length of double-stranded DNA (~50 nm). In contrast, the 32 nm stem displays more noticeable bending fluctuations, although it remains relatively straight overall. Analysis of the end-to-end distance between the arm tips shows a broad distribution. Notably, in about 10% of the configurations, the arms come close enough, that any proteins attached at the tips—assuming typical dimensions—would be able to interact with each other.

Working Principle of the Proximity Binding Assay for PROTAC Analysis

To demonstrate the working principle of the Y-structure for PROTAC analysis, we used a well-characterized system

https://doi.org/10.1021/acssensors.5c04944
ACS Sens. XXXX, XXX, XXX−XXX

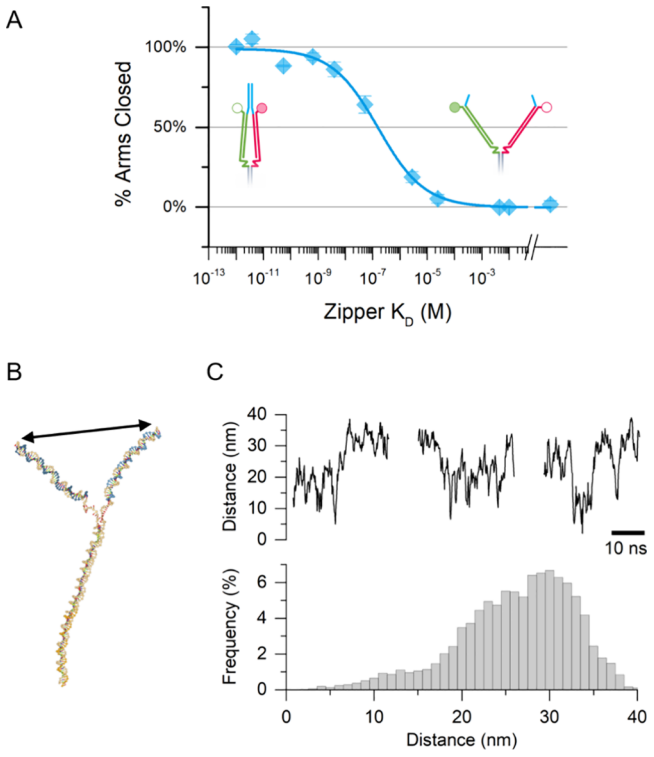

Figure 2. Characterization of Y-structure induced proximity. (A) Affinity calibration using DNA zippers with pre-determined binary K_d-values (Figure S1B–E). Sequence-complementary single stranded oligodeoxynucleotides (DNA-zippers), of variable lengths, ranging from 0 nt (right of axis break) to 15 nt (leftmost), are protruding from the swivel arms (shown in blue). The fraction of closed arms inferred from the FRET signal is plotted versus DNA-zipper affinities, which were measured separately (Figure S1). The half-closed midpoint is at 150 nM. (B,C) Results from oxDNA2 MD simulations. (B) Snapshot of a Y-structure configuration with arrows marking the end-to-end distance between 48 bp swivel arms (16 nm each). (C) Top: three representative time series of end-to-end distances extracted from 30 ns simulation runs. Bottom: End-to-end distance histogram, compiled from twelve 30 ns simulation runs. Additional snapshots and time traces are shown in Figure S1.

composed of VHL-EloB-EloC (VCB) as the E3 ligase substrate receptor and adaptor proteins, the BET bromodomain protein $BRD4^{BD2}$ as the target, and the bifunctional compounds AT1 and MZ1 as PROTACs.[12,24] MZ1 and AT1 are based on the same BRD4- and VHL-binding moieties (JQ1 and VH032) but feature a different linker and connection point on the VHL binder, PROTAC structures are shown in Scheme S2. To functionalize the Y-structure with ligase and target proteins, proteins were conjugated through NHS ester coupling to DNA strands that were complementary to the sequences of the red and green arms of the Y-structure, using off-the-shelf conjugation kits, and purified by ion exchange chromatography. The Y-structure was assembled before the sensing experiment by incubating DNA-protein conjugate strands with stem strands and subsequently immobilized on the sensor surface (the workflow for sensor regeneration is shown in Figure S2).

Binary interactions between PROTAC and target, and PROTAC and E3 ligase, were analyzed by functionalizing only one arm with a protein, while the other arm was double stranded but remained unmodified. Binding kinetics were followed in one of two colors: green fluorescence was excited and detected for $BRD4^{BD2}$ target, and alternatively red fluorescence was excited and detected for VCB ligase. In both cases, the quenching mode was used for detection of PROTAC binding (Figure 3A,C).

To measure PROTAC-mediated ternary complex formation, both arms of the Y-structure were functionalized with proteins, see Figure 3B. $BRD4^{BD2}$ target-conjugate was hybridized to the arm modified with the green dye, and VCB ligase-conjugate was hybridized to the red arm. Fluorescence was excited selectively in green only, while emission was measured in green and red simultaneously. Upon injection of PROTAC analyte, a mirror-like decrease in green fluorescence and a concomitant increase in red fluorescence are detected. The increase in red fluorescence in the ternary binding experiment (middle panel in Figure 3A) differs from the red signal observed in the binary binding experiments, because red fluorescence cannot be excited directly by the green illumination (cf. the flat line in left panel of Figure 3A), and it does not exhibit a quenching signature (right panel in Figure 3C). Therefore, we attribute the red emission to indirect excitation via green-to-red FRET, which results from a closing of the Y-structure as PROTACs interlink target and ligase proteins.

We cannot quantify molecular distances accurately, but we estimate from the emission intensities that the green and red dyes reside within 1–2 Förster radii of each other when the arms are closed. This corresponds to a distance of roughly 5–10 nm, which is reasonable considering the dimensions and the spatial arrangement of the molecules involved.

While the red fluorescence-increase results from FRET, the green fluorescence-decrease is caused by a convolution of two effects, namely, the direct quenching by the presence of MZ1 and the loss of green emission intensity due to FRET. Hence, the green signal reports binary and ternary binding, whereas the red, FRET-only signal selectively reports the formation and decay of the ternary complex.

Analysis of Binding Kinetics Determined with the Proximity Binding Assay and Comparison with SPR Values

The formation and decay of binary and ternary complexes involving MZ1 (Figure 3) and AT1 (Figure S3) can be described well by a Langmuir-like binding model (eq S1). Data were fitted globally for all concentrations without the need for mass-transport correction factors using mono-exponential functions $\propto \exp\{-(ck_{on} + k_{off})t\}$ and $\propto \exp\{-k_{off}t\}$ for the association and dissociation phases, respectively. To interpret the data, it is useful to consider the association and dissociation pathways underlying ternary complex formation and decay in the Y-structure proximity assay and SPR assay (see Scheme 2). The ternary rate constants, which are apparent when measured with a specific assay, are to be interpreted with respect to the transitions highlighted by the bold arrows in Scheme 2.

During the association phase in the Y-structure assay, the PROTAC (B) is injected over pre-immobilized target (A) and ligase (C). The ternary complex (ABC) can form via either of two intermediate binary complexes, AB or BC. However, these binary intermediates are not detected by the FRET readout, which is indicated by dashed lines in Scheme 2, as the Y-structure remains open in their presence. A high FRET signal is only observed upon formation of the ternary complex, which induces closure of the Y-structure arms (bold arrows in Scheme 2). The same principle applies during the dissociation phase: the

https://doi.org/10.1021/acssensors.5c04944
ACS Sens. XXXX, XXX, XXX–XXX

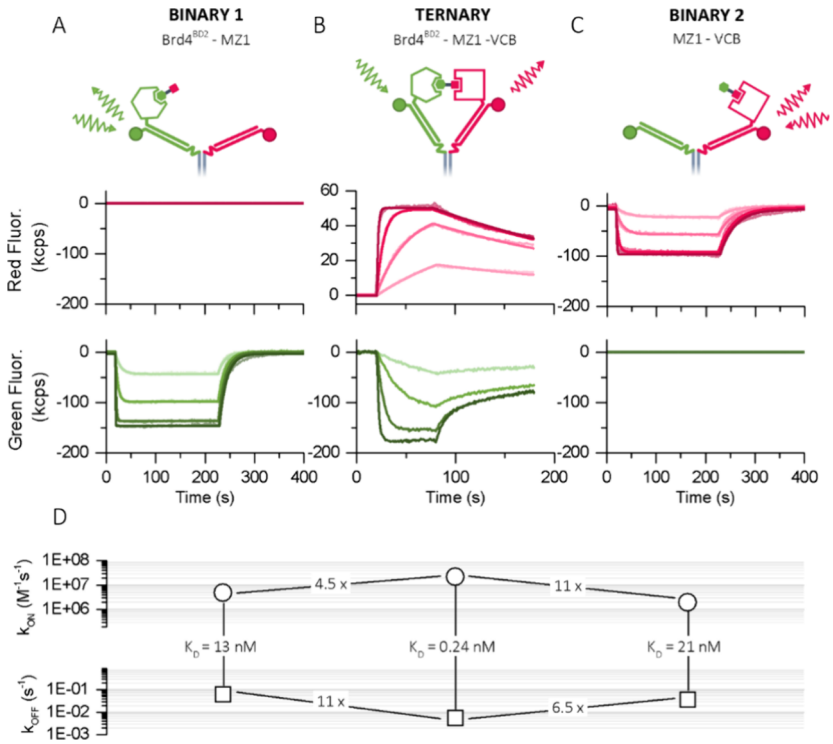

Figure 3. Proximity binding assay (PBA) with a DNA Y-nanostructure for the measurement of binary and ternary binding kinetics of bifunctional small molecules. (A) Binary binding of the PROTAC MZ1 to the POI BRD4^{BD2} results in a quenching of green fluorescence (FPS detection). MZ1 was injected at concentrations 4, 20, 100, and 500 nM at $T = 12$ °C. (B) Ternary complex formation involving MZ1 to BRD4^{BD2} and the E3 ligase VCB results in a quenching of green (FPS and FRET) and a simultaneous increase of red fluorescence (FRET). MZ1 was injected at concentrations of 0.16, 0.8, 4, 20 nM at $T = 25$ °C. (C) Binary binding of MZ1 to VCB results in the quenching of red fluorescence (FPS). MZ1 was injected at concentrations of 4, 20, 100, 500 nM at $T = 12$ °C. All measurements were performed in 1% DMSO. (D) Rate scale plot depicting association and dissociation rate constants (k_{on}, k_{off}), and the dissociation constant (K_d). Binary interactions with BRD4^{BD2} and with VCB are shown on the left and on the right, respectively, while ternary interaction constants (cf. Scheme 2, $k_{on}^{ter,PBA}$ and $k_{off}^{ter,PBA}$) are shown in the middle (corresponding to data from A to C).

ternary complex can decay via either binary intermediate. Once the ternary complex dissociates, the FRET signal drops immediately, but the assay does not distinguish which binary complex is involved in the dissociation, nor whether the PROTAC has completely dissociated from the Y-structure. Accordingly, the apparent on- and off-rate constants extracted from the FRET signal reflect ternary complex dynamics, while remaining agnostic to which binary intermediate is involved.

In a typical SPR assay,[12] only one protein—commonly the ligase (C)—is immobilized on the sensor surface (Scheme 2, bottom). The target protein (A) is pre-incubated with the PROTAC (B) at a concentration high enough to ensure that nearly all PROTAC molecules are bound to the target (i.e., $c_A \gg K_d^{AB}$, for example, 2 μM BRD4[12]). During the association phase, the AB complex is injected over the immobilized ligase C, allowing it to form the ternary complex (ABC). In the dissociation phase, two possible pathways may contribute to the signal decay: (1) direct dissociation of AB from C, or (2) dissociation of A from the BC complex, followed by dissociation of B from C. The SPR signal does not distinguish between these pathways, as both result in a decrease in response.

According to Scheme 2, the ternary on-rate constants determined with the PBA and SPR assays are expected to differ between the assays, whereas the ternary off-rate constants should be similar. In SPR, the specific association pathway being measured depends on which protein is immobilized, and which complex is preincubated, thereby isolating a single route to ternary complex formation. In the SPR format, pre-saturation ensures that ternary complex formation proceeds predominantly via the AB + C → ABC transition, whereas in the Y-structure assay, both AB and BC intermediates are accessible, leading to an apparent ternary association rate constant that reflects the combination of both accessible pathways. The term 'apparent' is used here to indicate that the observed rate constants reflect the transitions that are experimentally accessible in each assay geometry, not intrinsic microscopic rates. We emphasize that this difference in apparent rate constants does not indicate that one method outperforms the other. Instead, the two assays report on different kinetic observables: SPR isolates a defined association pathway by pre-saturating one binding interface, while the Y-structure assay measures the effective rate of ternary complex formation under induced-proximity conditions where both pathways are accessible. Viewed in this way, the two techniques are complementary, providing distinct and non-redundant mechanistic information about ternary complex assembly.

Ternary off-rate constants, by comparison, are expected to be similar for the two assays, as both are agnostic to the specific binary intermediates involved in ternary complex dissociation. As such, the measured off-rate constants reflect a convolution of multiple pathways: $k_{off}^{ABC \rightarrow AB + C}$ and $k_{off}^{ABC \rightarrow A + BC}$. In SPR,

https://doi.org/10.1021/acssensors.5c04944
ACS Sens. XXXX, XXX, XXX–XXX

$k_{off}^{BC\rightarrow B+C}$ may also contribute, though to a lesser extent, due to the lower molecular weight of B.

Consistent with this, both assays yield comparable ternary off-rate constants for MZ1 and AT1 (Table 1), with MZ1 (5×10^{-3} s^{-1}) conferring greater ternary complex stability than AT1 (25×10^{-3} s^{-1}). The ternary on-rate constants obtained with the Y-structure are substantially higher than those measured by SPR, likely due to the two available association pathways in the Y-structure compared to only one in SPR. The relative differences in on-rate and off-rate constants between PROTACs measured using the Y-structure and SPR are comparable across both methods, resulting in the same ranking of compounds.

In their binary interactions with $BRD4^{BD2}$, both PROTACs exhibit similar kinetics and affinities. In contrast, their affinities for VCB are weaker and differ markedly between MZ1 and AT1, with MZ1 displaying a faster association rate. These trends are consistent with SPR data; however, the rates measured by fluorescence are generally 2−3 times higher (except for AT1-VCB). These discrepancies may arise from differences in experimental protocols. Although we adopted conditions similar to those used in a previous SPR study,[12] the immobilization methods differed. In that SPR work, VCB was immobilized via a site-specific method involving C-terminal biotin capture on a streptavidin-modified dextran matrix, while BRD4 was labeled non-specifically using NHS-biotin. In the present study, we employed stoichiometrically purified protein-DNA conjugates (Figures S27−S29) linked via non-specific NHS chemistry and hybridized to DNA molecules tethered to gold surfaces. Further, protein immobilization densities varied: less than 10^9 molecules/mm^2 in Y-structure experiments (equivalent to app. 100 RUs) compared to 2000−3000 RUs in SPR experiments. Lower immobilization densities can lead to the observation of faster kinetics and different immobilization methods (site-specific capture vs. non-specific coupling through lysines) can also influence the quantification of rate constants.

To better understand factors affecting the stability and kinetics of the MZ1 interaction, we investigated the influence of both solvent conditions and temperature. DMSO, commonly used at low concentrations to solubilize small-molecule compounds, was present at 1% in previous SPR studies and was therefore included at the same concentration in the experiments shown in Figures 3 and S7. As bromodomains have been reported to be sensitive to inhibition by DMSO,[26,27] we conducted comparative experiments in the absence of DMSO (Figures S5−S7, and Tables S1−S3). These revealed that 1% DMSO significantly interferes with the MZ1−$BRD4^{BD2}$ interaction, reducing the association rate by approximately three-fold. The dissociation rate constant was only slightly elevated, indicating a minor destabilizing effect. In contrast, the interaction between MZ1 and VCB remained unaffected by the presence of DMSO. We further examined the effect of temperature on MZ1−$BRD4^{BD2}$ binding in the range of 12−25 °C (Figure S6). While the on-rate exhibited minimal change across this temperature span, we observed a pronounced destabilization of the complex, manifested as a four-fold increase in the off-rate constant at elevated temperatures. Similar temperature effects have been reported for other small molecule−protein interactions in SPR studies.[28]

At high PROTAC concentrations, the onset of autoinhibition of ternary complex formation is observed (Figure S4)—a phenomenon commonly known as the "hook effect". This effect, frequently seen in ternary complex formation, is characterized by a hook-shaped decrease in signal intensity with increasing analyte concentration.[29] At elevated concentrations, two PROTAC molecules can simultaneously bind to the same Y-structure, preventing proper ternary complex formation and keeping the structure in an open conformation.

SPR measurements revealed a decrease in the dissociation constant K_d for ternary complexes compared to their binary counterparts, a phenomenon known as positive cooperativity. This effect is quantified by the cooperativity factor, α, defined as $\alpha = K_d^{bin}/K_d^{ter,SPR}$. Cooperativity values for MZ1 and AT1 were determined using the SPR workflow outlined in Scheme 2, yielding $\alpha_{MZ1} = 48$ and $\alpha_{AT1} = 9$ by selecting K_d^{bin} of the PROTAC-VCB interaction as the binary reference (α values are mean values from sensorgrams in the Supporting Information of the SPR study)[12].

Similarly, a decrease in K_d was observed for ternary complexes analyzed using the Y-structure proximity binding assay. To capture this effect, we introduce the factor β, defined as $\beta = K_d^{bin}/K_d^{ter,PBA}$, where $K_d^{ter,PBA}$ represents the ternary complex dissociation constant measured via the proximity binding assay with the Y-structure. This yielded $\beta_{MZ1} = 88$ and $\beta_{AT1} = 33$, notably higher than corresponding α-values. The discrepancy between α and β can be attributed to differences in immobilization configurations between the two assays. In the SPR format, where only one protein is immobilized, analytes dissociate irreversibly upon unbinding. In contrast, the Y-structure positions both binding partners in close proximity on the same surface, enabling a rebinding effect that mimics avidity. Upon partial dissociation of the ternary complex, an intermediate binary complex may transiently form and quickly re-engage, effectively reducing the ternary $K_d^{ter,PBA}$. This avidity-driven rebinding depends on the spatial and dynamic properties of the Y-structure, including its flexibility, the collision frequency of its arms, and the nature of the linkages connecting the proteins to the Y-structure. Thus, the β-value reflects not only molecular cooperativity but also the contribution of structural proximity effects inherent to the Y-structure assay.

Screening of Ternary and Binary Interactions of PROTACs Binding to $BRD4^{BD2}$ and CRBN

Next, we performed a screen that simultaneously measures ternary and binary interactions, which is shown in Figure 4. The target was $BRD4^{BD2}$, and the ligase was cereblon-DDB1 (CRBN), because CRBN is of great interest in ongoing drug discovery projects but has been difficult to handle in conventional biophysical assays, exhibiting poor stability and non-specific interactions on SPR surfaces. A 96 well plate was filled with nineteen compounds (Scheme S2) at fixed concentrations of 20 nM: 6 bifunctional molecules known to engage both $BRD4^{BD2}$ and CRBN simultaneously, 9 compounds (bifunctional molecules or monovalent ligands) known to engage either $BRD4^{BD2}$ or CRBN individually, and 2 negative control compounds, which are listed in Table S19. Four replicates were performed within the same assay to test for repeatability. 384 real-time binding signals were recorded simultaneously in two colors from two spots during 96 injections. Spot 1 was functionalized with a Y-structure featuring $BRD4^{BD2}$ on the green arm and CRBN on the red arm, and 192 sensorgrams are shown in Figure 4 (96 red and 96 green signals). Spot 2 was

https://doi.org/10.1021/acssensors.5c04944
ACS Sens. XXXX, XXX, XXX−XXX

Table 1. Binding Constants of MZ1 and AT1 PROTACs[a]

solute analyte	immobilized protein	method	k_{on} (1E6 M^{-1} s^{-1})	k_{off} (1E-3 s^{-1})	K_d (nM)
Binary interactions (T = 12 °C)					
MZ1	$BRD4^{BD2}$	this work[b]	4.9 ± 1.5	61 ± 2	13 ± 3
		SPR[12]	2.6	20	7.5
	VCB	this work[b]	2.0 ± 0.9	35 ± 1	21 ± 8
		SPR[12]	0.7 ± 0.1	19 ± 4	29 ± 3
AT1	$BRD4^{BD2}$	this work[b]	5.0 ± 1.1	58 ± 17	11 ± 1
		SPR[12]	2.1	19	9
	VCB	this work[b]	0.3 ± 0.1	41 ± 3	140 ± 12
		SPR[12]	0.6 ± 0.1	60 ± 20	110 ± 40
solute analyte(s)	**immobilized protein(s)**	**method**	$k_{on}^{ter,PBA/SPR}$ (1E6 M^{-1} s^{-1})	$k_{off}^{ter,PBA/SPR}$ (1E-3 s^{-1})	$K_d^{ter,PBA/SPR}$ (nM)
Ternary interactions (T = 25 °C); rate constants are labelled PBA or SPR, corresponding to the transitions indicated by the bold arrows in Scheme 2					
MZ1	VCB, $BRD4^{BD2}$	PBA, this work[b]	22.1 ± 0.1	5.4 ± 0.1	0.24 ± 0.03
MZ1, preincub. w. 2 μM BRD4	VCB	SPR[12,c]	8.1 ± 0.1	4.9 ± 0.1	0.61 ± 0.02
AT1	VCB, $BRD4^{BD2}$	PBA, this work[b]	5.9 ± 0.1	25.3 ± 0.6	4.3 ± 0.1
AT1, preincub. w. 2 μM BRD4	VCB	SPR[12,c]	1.7 ± 0.2	20 ± 2	12 ± 3

[a]Interacting with $BRD4^{BD2}$ and VCB ligase substrate receptor on a Y-structure determined by the proximity binding assay (PBA). Binary on- and off-rate constants are analyzed by FPS (quenching, cf. A and C in Figures 3 and S3), ternary on- and off-rate constants are analyzed via FRET (B in Figures 3 and S3). Literature SPR values are listed for comparison. See Scheme 2 for the interpretation of rate constants determined by the PBA and SPR assays. [b]For comparison, experiments were performed at the same temperatures, flow rates, association/dissociation times, and DMSO concentration of 1%, which were used in a previous SPR study[12]: AT1-$BRD4^{BD2}$: T = 12 °C, flow rate = 100 μL/min, 200 s/300 s; AT1-VCB: 12 °C, 50 μL/min, 120 s/300 s; AT1-$BRD4^{BD2}$-VCB: 25 °C, 100 μL/min, 100 s/80 s; MZ1-$BRD4^{BD2}$: 12 °C, 100 μL/min, 200 s/300 s; MZ1-VCB: 12 °C, 50 μL/min, 60 s/300 s; MZ1-$BRD4^{BD2}$-VCB: 25 °C, 100 μL/min, 60 s/80 s. Immobilization conditions differed between the SPR and Y-structure assays, see text. The values shown represent the mean ± SD of at least three independent experiments. [c]Mean values were calculated from original sensorgrams in the Supporting Information of ref [12] (Figures S3 and S8 in ref [12]).

functionalized with a Y-structure with $BRD4^{BD2}$ target only and 2x96 sensorgrams are shown in Supporting Figure S8. This configuration enables the simultaneous measurement of ternary complex formation on spot 1 as well as binary kinetics on spot 2 within the same experiment. The biosensor chip was regenerated and freshly functionalized at the end of each row, i.e., every 12 analyte injections. Over the course of 8 regenerations during the measurement of one well plate, 15 pmol of CRBN and 30 pmol of $BRD4^{BD2}$ were consumed. PROTACs that induce the formation of a ternary complex between $BRD4^{BD2}$ and CRBN, i.e., ARV-825 and compounds of the dBET family, can easily be identified in Figure 4A by a mirror-like signal response, that is, an increase in the red FRET signal and a concomitant decrease of the green signal. Compounds that only interact with $BRD4^{BD2}$ but not with CRBN, for example MZ1 or MZ2, exhibit a decrease in green fluorescence, but no signal change in red fluorescence. Negative controls do not show any signal change, in either the green or the red channels. Simultaneous measurements on spot 2, which is only functionalized with $BRD4^{BD2}$, validate binary interactions with the target protein and serve as a real-time reference (Figure S8).

The screening of the selected compounds yielded six ternary hits: ARV-825, ARV-825(2), dBET1, dBET6, dBET6(2), and dBET260 were identified as PROTACs, which interlink target and ligase. Of note, PROTACs marked with the suffix "(2)" had been obtained from different manufacturers and were exchanged between the authors of this study in a blinded manner. They were consistently identified as hits and their kinetics agree with the compounds without a suffix (see below), which corroborates a good reproducibility of the assay. The red signal changes are reproducible from the first to the last row, suggesting a satisfying stability of the functionalized Y-structure over the measurement time of 22 h. Binary binding to $BRD4^{BD2}$ was observed for nine small molecules: MZ1, MZ2, MZ4, AT1, and cisMZ1 feature a (+)-JQ1 moiety, which binds to BET proteins, including $BRD4^{BD2}$. They are PROTACs which recruit VHL, but they do not bind CRBN. The BET bromodomain inhibitor (+)-JQ1 shows a detectable signal in green, demonstrating the high sensitivity of the assay to analyze protein-small molecule binding. Binary binding signals to $BRD4^{BD2}$ are also observed for OTX015, ARV-771, and ZXH-3-26. Pomalidomide (Pom) targets CRBN, but does not generate a signal, as binary binding to the E3 ligase substrate receptor is not read-out in the used assay setup. To confirm that the interaction of Pom with CRBN is detectable, it was measured in a separate assay and a K_d of 577 nM was obtained (Figure S9). As expected, VH032 did not give a signal, as it is a monovalent compound that targets VHL alone, and indeed VHL was not present in the assay.

Hit maps, which show ternary versus binary binding signals, are presented in Figure 4I,J. Ternary binding activity is inferred from the red FRET signal amplitude on spot 1, while binary binding activity to the target is inferred from the green fluorescence amplitude on spot 2, where only $BRD4^{BD2}$ had been immobilized. PROTACs with ternary binding capability (ARV-825 and dBET family) can immediately be identified and discriminated from compounds featuring only binary interactions from the relative fluorescence changes plotted in Figure 4I. To assess the statistical significance of the identified hits with ternary and binary binding activity, fluorescence data were analyzed by a two-sample t-test with Welch correction, in which the mean values and standard deviations of red and green signals of each compound (n = 4) were compared with blank injections (n = 16). The resulting P-values are plotted in a hit confidence map in Figure 4J. The confidence map is divided into four hit quadrants, namely, ternary and binary,

https://doi.org/10.1021/acssensors.5c04944
ACS Sens. XXXX, XXX, XXX−XXX

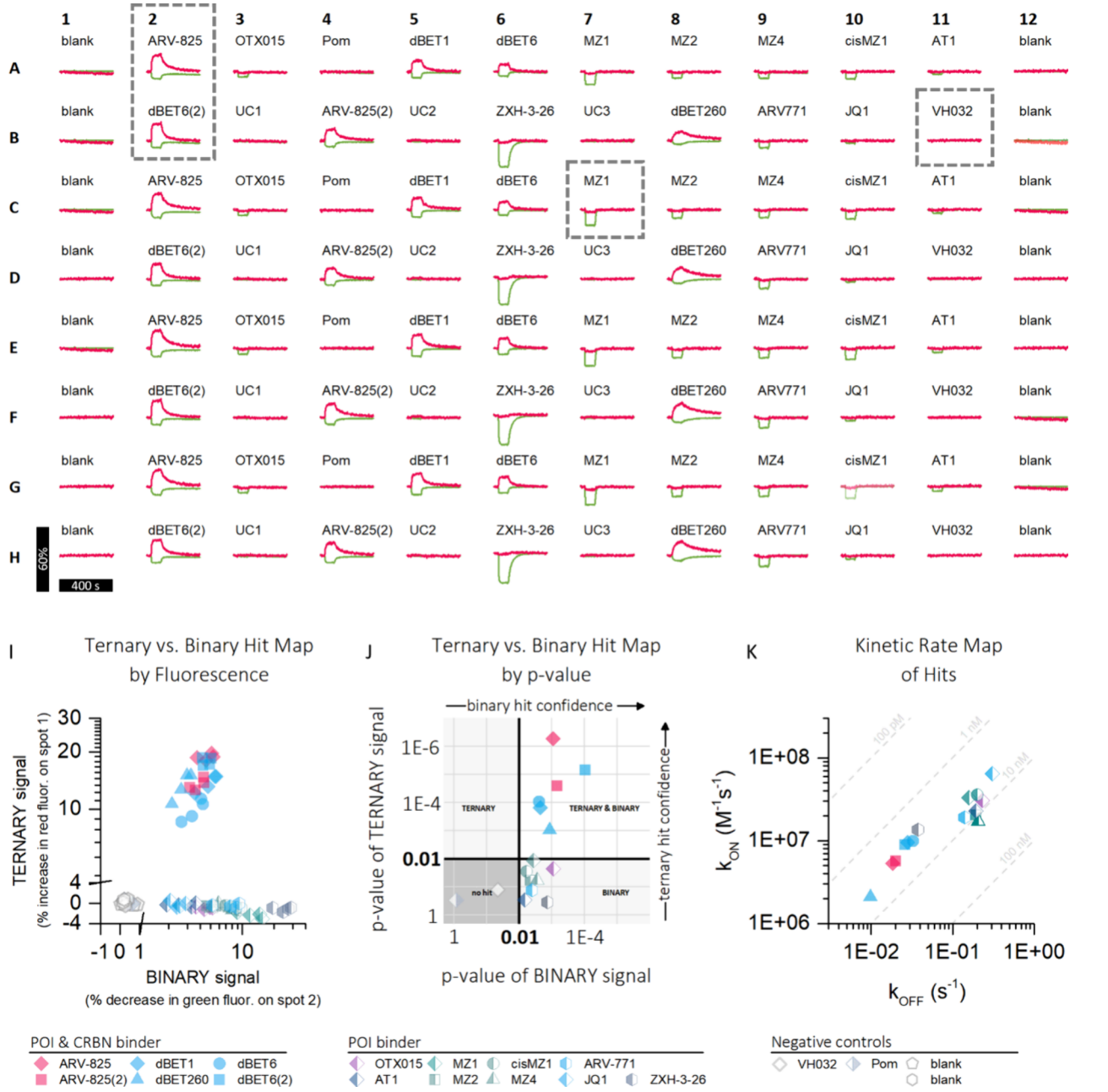

Figure 4. PROTAC screen of 96 samples, measured in two colors on two detection spots. PROTACs forming ternary complexes are depicted as full symbols, binary binders are half full symbols, and negative controls are empty symbols. (A–H) Fluorescence sensorgrams of PROTACs interacting with CRBN (red signal) and $BRD4^{BD2}$ (green signal): ARV-825, ARV-825(2), dBET1, dBET6, dBET6(2), and dBET260 PROTACs form ternary complexes between CRBN, PROTAC, and $BRD4^{BD2}$, identifiable by the red FRET signal increase and concomitant quenching of the green signal. Shown are signals from spot 1 with a Y-structure functionalized with $BRD4^{BD2}$ and CRBN. Data from spot 2, functionalized with $BRD4^{BD2}$ only, are shown in Supporting Figure S8. (I) Ternary vs. binary hit map by fluorescence: percent increase in red fluorescence on spot 1 vs. percent decrease in green fluorescence on spot 2 for all 96 samples. (J) Ternary vs. binary hit map by *P*-value: *P*-values of red FRET signals are plotted vs. *P*-values of green signals (two-sample *t*-test with Welch correction, $n = 4$ for each compound, referenced to $n = 16$ blank traces). (K) Kinetics rate map: mean k_{on} rates versus mean k_{off} rates ($n = 4$), as analyzed before from single exponential functions (cf. text and SI eq 1), dashed iso-affinity lines are plotted for $K_d = 0.1$, 1, 10, and 100 nM. Ternary rate constants (cf. Scheme 2, $k_{on}^{ter,PBA}$ and $k_{off}^{ter,PBA}$) are full symbols, binary rate constants are half full symbols. Measurements were performed at 25 °C in the absence of DMSO.

ternary, binary, and no hit, by selecting cut-off values of $P < 0.01$. It shows that ternary and binary binders are correctly identified in the screen and can be discriminated from binary binders and negative controls with satisfying statistical significance.

Kinetic Hit Characterization and Validation

Kinetic rate constants k_{on} and k_{off}, and K_d values can be analyzed directly from the real-time sensorgrams obtained from the screening assay. The kinetics of ternary and binary hits

https://doi.org/10.1021/acssensors.5c04944
ACS Sens. XXXX, XXX, XXX–XXX

can be fitted well with mono-exponential functions, as shown in Figures S10−S24 (Tables S4−S18). Mean values and standard deviations from four replicates are summarized in Table S19 and k_{on} and k_{off} rate constants are plotted in the rate map shown in Figure 4K. Relative standard deviations are 6% on average (maximal 21%) for ternary rate constants, and 13% on average (maximal 34%) for binary rate constants, which indicates good repeatability. Of note, the rates of compounds ARV-825 and ARV-825(2) as well as dBET6 and dBET6(2), which were obtained from different manufacturers, superimpose well in the rate map.

The rate map illustrates why it is insightful to measure kinetic binding data instead of inferring steady state K_d values from a titration assay. While most compounds feature very similar K_d values and approximately align along an iso-affinity line in the single-digit nanomolar K_d range, their k_{on} and k_{off} values are very different. For instance, dBET260 features much slower ternary on- and off-rate constants than dBET6, yet both have comparable K_d values. Also, the ternary binding rate constants of PROTACs (full symbols) are lower than the rate constants of binary binding of their individual POI binding moieties (half-full symbols), although their K_d-values are similar (compare, e.g., ARV-825 to OTX015 or dBET6 to (+)-JQ1). Dissimilar binding kinetics may result in different pharmacodynamics, and thus the selection of hits according to their binding kinetics can be valuable for drug development.

For hit validation, we characterized the ternary binders ARV-825 and dBET6, which were designed by the Crews[8] and Bradner[30] laboratories, respectively. The PROTACs are interesting for comparison, as they bind CRBN via the same ligase-binding-moiety, pomalidomide, yet feature different target-binding-moieties, namely OTX015 in the case of ARV-825, and (+)-JQ1 in the case of dBET6. Long linkers connect the moieties of both PROTACs: ARV-825 has a hydrophilic ethylene glycol EG_4 linker, while dBET6 has an alkane C_8 linker.

A detailed analysis of ternary and binary interactions of ARV-825 and dBET6 with $BRD4^{BD2}$ and CRBN—including additional sensorgrams and enhancement factor calculations—is provided in the Supporting Information (Figures S25 and S26, Tables S19−S21). Ternary rate constants obtained from sensorgrams with multiple analyte injections agree with screening data that were recorded using a single compound concentration (cf. Tables S19 and S20), which substantiates the validity of kinetic analyses from screening data. Sensorgrams of ternary complex formation (Figures S25 and S26) suggest a sequential binding mechanism in which the PROTAC first engages $BRD4^{BD2}$ and subsequently recruits CRBN, with ternary complexes exhibiting longer lifetimes than the corresponding binary complexes, particularly for ARV-825.

For binary interactions, enhancement factors α^* were calculated to quantify how non-cognate PROTAC moieties influence the binding of the cognate binding motifs (Table S21). Non-cognate moieties are found to stabilize the binding of both PROTACs to CRBN and $BRD4^{BD2}$, but the association rate constants for $BRD4^{BD2}$ binding are reduced.

Selectivity among BET family members and their bromodomains is an important consideration for the clinical exploitation of PROTACs. Because BET bromodomains are highly conserved, many BET inhibitors and derived PROTACs act as pan-BET binders with limited discrimination.[31−35] However, ternary complex formation can introduce an additional layer of selectivity beyond binary binding.[12,24,36−38] To demonstrate the applicability of the presented method for probing such selectivity, we analyzed ternary complex formation of ARV-825 with CRBN and the BD1 and BD2 bromodomains of BRD2, BRD3, BRD4, and BRDT (Figure S27).

For BRD2, BRD3, and BRD4, ternary complex formation shows nearly identical kinetics over the tested ARV-825 concentration range (0.8−100 nM), with binding rate constants indistinguishable within experimental error (Table S22). Minor differences between bromodomains are observed only in the presence of CRBN, with slightly faster association to BD1 and slower dissociation from BD2, whereas the corresponding binary interactions show no such trend (Figure S28, Table S23). These results confirm that ARV-825 acts as a promiscuous pan-BET binder without discrimination among BRD2, BRD3, and BRD4. Notably, however, no interaction is detected with BD2 of BRDT up to 100 nM.

■ DISCUSSION AND CONCLUSIONS

The Y-structure assay positions two proteins at defined relative stoichiometry and spatial proximity, which allows ternary complex formation to be monitored directly via a FRET signal. This configuration inherently increases the probability of encounter between the binding partners and therefore can introduce proximity-driven avidity. As a consequence, the apparent ternary affinity in this assay reflects not only intrinsic molecular cooperativity but also structure-dependent rebinding effects. The degree to which this avidity contributes depends on linker flexibility, arm dynamics, and the effective local concentration created by the Y-structure geometry.

It is therefore important that the kinetic constants measured here are interpreted as assay-specific apparent rate constants, rather than absolute microscopic rate constants. In contrast to SPR, where pre-saturation of one binary interaction isolates a single association pathway, the Y-structure assay allows both AB → ABC and BC → ABC pathways to contribute to the observed association rate. These two assay formats are thus complementary: SPR reports kinetics along a defined pathway, whereas the Y-structure reports effective rates under conditions where both pathways are accessible.

The induced-proximity configuration also differs from the situation in cells. In degradation pathways, ternary complex formation is influenced by additional factors including protein localization, conformational states, ubiquitination machinery accessibility, and cellular concentration regimes. For these reasons, the Y-structure assay is not intended as a direct predictor of degradation efficacy, but rather as a readout of the kinetic competence of ternary complex assembly.

It has been shown that ternary complex stability, not just binary affinity, can be important for achieving efficient degradation[16,24,39,40] and that ternary complex half-life correlates with degradation efficiency and initial rate of degradation,[12,14,39] but cellular degradation additionally depends on downstream events beyond ternary complex lifetime.

The assay described here probes ternary complex formation, which is a necessary, but not sufficient condition for ubiquitination. For example, dBET6 has been reported to be a better degrader than dBET1,[30,41] because of better intracellular permeability and stability,[30] yet the binding parameters analyzed here are similar. Moreover, degradation concentrations from in vitro cellular assays must be compared carefully, because

https://doi.org/10.1021/acssensors.5c04944
ACS Sens. XXXX, XXX, XXX−XXX

DC_{50} values (half-maximal degradation concentration) depend on the type of cell, type of functional assay, target version, and the incubation time.[13,42] Nonetheless, the literature agrees for degradation of BRD4 via CRBN that ARV-825 is more potent than dBET6, and for degradation via VCB that MZ1 is more potent (yet less BRD4-selective) than AT1, albeit reported DC_{50} values vary (ARV-825: <1 nM for Burkitt's lymphoma cells,[8] 0.6 nM for 22RV1,[43] 1 nM for NAMALWA,[44] 1 nM for CA46,[44] 5 nM for Jurkat[45] and Molt,[45] 26 nM for 6 T-CEM[45]; dBET6: app. 50 nM for HEK293T,[36] app. 100 nM for 661W[46], <500 nM for glioblastoma[47]; MZ1: app. 3 nM for HeLa[48], 23 nM (K_m) for Flp293T[42]; AT1: 10−100 nM for HeLa[24]). The same trend is observed for the ternary complex half-life, but not the affinity, in the proximity binding assay. For both ligases, the PROTACs with the longer half-lives are also the better degraders ($t_{1/2}^{ARV-825} = 2 \times t_{1/2}^{dBET6}$, $t_{1/2}^{MZ1} = 3 \times t_{1/2}^{AT1}$), while almost identical $K_d^{ter,PBA}$ values were measured for ARV-825 and dBET6, which corroborates previous findings[12] that binding kinetics might be useful indicators for predicting degradation success. With the proximity binding assay, PROTACs with different ternary complex half-lives could be readily distinguished in a screening context, despite exhibiting nearly identical dissociation constants.

While a strong proximity effect may alter the apparent kinetics, it can be desirable and open new strategies for the discovery of low-affinity compounds. Compounds from a fragment library or molecular glues, which interact only weakly with target proteins, often cannot be identified with conventional screening methods, as at least two of three ternary interactants would need to be incubated at impractically high concentrations. A strong proximity effect can induce ternary complex formation already for weak interactants and enable the identification of otherwise undetectable drug candidates.

Taken together, the Y-structure assay is most useful for (i) comparing ternary complex kinetics across structurally related PROTACs, (ii) identifying compounds capable of forming kinetically stable ternary complexes, and (iii) high-throughput screening of ternary engagement. It should, however, be interpreted in conjunction with complementary methods such as SPR and cellular degradation assays to obtain a full understanding of PROTAC performance.

The assay may be applied in the discovery of various candidates for proximity inducing therapeutic modalities,[49] such as PROTACs, molecular glues,[50] regulated induced proximity targeting chimeras (RIPTACs),[51] or transcriptional chemical inducers of proximity (TCIPs).[52] We anticipate that the multivariate information on ternary and binary complex formation provided by the proximity binding assay, in conjunction with the ability to screen many compounds at low sample consumption, will aid the characterization and optimization of future PROTACs, molecular glues, and other bispecific proximity-inducing matchmakers.

■ ASSOCIATED CONTENT

Supporting Information

The Supporting Information is available free of charge at https://pubs.acs.org/doi/10.1021/acssensors.5c04944.

Additional reaction pathways, materials and methods, chemical structures, workflow schematics, sensorgrams, and chromatograms (PDF)

■ AUTHOR INFORMATION

Corresponding Authors

Stefan Geschwindner – *Protein, Structure and Biophysics, Discovery Sciences, BioPharmaceuticals R&D, AstraZeneca, 431 83 Mölndal, Sweden*; orcid.org/0000-0002-2154-8345; Email: stefan.geschwindner@astrazeneca.com

Alessio Ciulli – *Centre for Targeted Protein Degradation, School of Life Sciences, University of Dundee, 1 James Lindsay Place, DD1 5JJ Dundee, U.K.*; orcid.org/0000-0002-8654-1670; Email: a.ciulli@dundee.ac.uk

Ulrich Rant – *Dynamic Biosensors GmbH Germany, Perchtinger Str. 8-10, 81379 Munich, Germany; Kurt-Schwabe-Institute for Sensor Technologies, Kurt-Schwabe-Strasse 4, 04376 Waldheim, Germany; University of Technology Dresden, 01069 Dresden, Germany*; orcid.org/0000-0002-6100-828X; Email: ulrich.rant@tu-dresden.de

Authors

Irene Ponzo – *Dynamic Biosensors GmbH Germany, Perchtinger Str. 8-10, 81379 Munich, Germany*

Alice Soldà – *Dynamic Biosensors GmbH Germany, Perchtinger Str. 8-10, 81379 Munich, Germany*

Charlotte Crowe – *Centre for Targeted Protein Degradation, School of Life Sciences, University of Dundee, 1 James Lindsay Place, DD1 5JJ Dundee, U.K.*; orcid.org/0000-0003-2068-8255

Göran Dahl – *Protein, Structure and Biophysics, Discovery Sciences, BioPharmaceuticals R&D, AstraZeneca, 431 83 Mölndal, Sweden*

Tereza Jahodová – *Dynamic Biosensors GmbH Germany, Perchtinger Str. 8-10, 81379 Munich, Germany*

Andreas Heerwig – *Kurt-Schwabe-Institute for Sensor Technologies, Kurt-Schwabe-Strasse 4, 04376 Waldheim, Germany*

Complete contact information is available at: https://pubs.acs.org/doi/10.1021/acssensors.5c04944

Author Contributions

‡I.P. and A.S. contributed equally to this work. The manuscript was written and edited through contributions from all authors. I.P., A.S., and T.J. carried out biosensor experiments. C.C. and G.D. prepared/provided proteins and small molecules. Data were analyzed by I.P., T.J., A.S., U.R., reviewed and discussed by all authors. U.R., A.S., A.C., and S.G. planned and supervised the project. All authors have given approval to the final version of the manuscript.

Notes

The authors declare the following competing financial interest(s): I. P., A. S., T. J. and U. R. are employed at Dynamic Biosensors which commercializes the heliX® biosensors used in this study. The Ciulli laboratory receives or has received sponsored research support from Almirall, Amgen, Amphista Therapeutics, Boehringer Ingelheim, Eisai, Merck KGaA, Nurix Therapeutics, Ono Pharmaceutical and Bio-Techne (Tocris). A.C. is scientific cofounder and shareholder of Amphista Therapeutics, a company that is developing targeted protein degradation therapeutic platforms. A.C. is on the Scientific Advisory Boards of ProtOS Bio and TrimTech Therapeutics. The remaining author(s) declare no competing interests.

https://doi.org/10.1021/acssensors.5c04944
ACS Sens. XXXX, XXX, XXX−XXX

■ ACKNOWLEDGMENTS

I.P. received funding from the European Union Horizon 2020 Research and Innovation Programme under the Marie Sklodowska-Curie Grant Agreement No. 765266 (LightDyNAmics). C.C. was funded by a PhD studentship from the UK Medical Research Council (MRC) under the Industrial Cooperative Awards in Science & Technology (iCASE) doctoral training program (MR/R015791/1). T.J. received funding from the European Union's MSCA Doctoral network Horizon Europe program Grant Agreement Number 101119951 (ECLectic).

■ ABBREVIATIONS

TPD	targeted protein degradation
PROTAC	proteolysis targeting chimera
POI	protein of interest
CRBN	Cereblon-DDB1
VHL	von Hippel-Lindau
FRET	fluorescence energy transfer
FPS	fluorescence proximity sensing

■ REFERENCES

(1) Sakamoto, K. M.; Kim, K. B.; Kumagai, A.; Mercurio, F.; Crews, C. M.; Deshaies, R. J. Protacs: Chimeric Molecules That Target Proteins to the Skp1−Cullin−F Box Complex for Ubiquitination and Degradation. *Proc. Natl. Acad. Sci. U. S. A.* **2001**, *98* (15), 8554–8559.

(2) Békés, M.; Langley, D. R.; Crews, C. M. PROTAC Targeted Protein Degraders: The Past Is Prologue. *Nat. Rev. Drug Discov.* **2022**, *21* (3), 181–200.

(3) O'Brien Laramy, M. N.; Luthra, S.; Brown, M. F.; Bartlett, D. W. Delivering on the Promise of Protein Degraders. *Nat. Rev. Drug Discov.* **2023**, *22* (5), 410–427.

(4) Marei, H.; Tsai, W.-T. K.; Kee, Y.-S.; Ruiz, K.; He, J.; Cox, C.; Sun, T.; Penikalapati, S.; Dwivedi, P.; Choi, M.; Kan, D.; Saenz-Lopez, P.; Dorighi, K.; Zhang, P.; Kschonsak, Y. T.; Kljavin, N.; Amin, D.; Kim, I.; Mancini, A. G.; Nguyen, T.; Wang, C.; Janezic, E.; Doan, A.; Mai, E.; Xi, H.; Gu, C.; Heinlein, M.; Biehs, B.; Wu, J.; Lehoux, I.; Harris, S.; Comps-Agrar, L.; Seshasayee, D.; De Sauvage, F. J.; Grimmer, M.; Li, J.; Agard, N. J.; De Sousa, E; Melo, F. Antibody Targeting of E3 Ubiquitin Ligases for Receptor Degradation. *Nature* **2022**, *610* (7930), 182–189.

(5) Pettersson, M.; Crews, C. M. PROteolysis TArgeting Chimeras (PROTACs)—Past, Present and Future. *Drug Discov. Today: Technol.* **2019**, *31*, 15–27.

(6) Bondeson, D. P.; Mares, A.; Smith, I. E. D.; Ko, E.; Campos, S.; Miah, A. H.; Mulholland, K. E.; Routly, N.; Buckley, D. L.; Gustafson, J. L.; Zinn, N.; Grandi, P.; Shimamura, S.; Bergamini, G.; Faelth-Savitski, M.; Bantscheff, M.; Cox, C.; Gordon, D. A.; Willard, R. R.; Flanagan, J. J.; Casillas, L. N.; Votta, B. J.; Den Besten, W.; Famm, K.; Kruidenier, L.; Carter, P. S.; Harling, J. D.; Churcher, I.; Crews, C. M. Catalytic in Vivo Protein Knockdown by Small-Molecule PROTACs. *Nat. Chem. Biol.* **2015**, *11* (8), 611–617.

(7) Diehl, C. J.; Ciulli, A. Discovery of Small Molecule Ligands for the von Hippel-Lindau (VHL) E3 Ligase and Their Use as Inhibitors and PROTAC Degraders. *Chem. Soc. Rev.* **2022**, *51* (19), 8216–8257.

(8) Lu, J.; Qian, Y.; Altieri, M.; Dong, H.; Wang, J.; Raina, K.; Hines, J.; Winkler, J. D.; Crew, A. P.; Coleman, K.; Crews, C. M. Hijacking the E3 Ubiquitin Ligase Cereblon to Efficiently Target BRD4. *Chem. Biol.* **2015**, *22* (6), 755–763.

(9) Yamamoto, J.; Ito, T.; Yamaguchi, Y.; Handa, H. Discovery of CRBN as a Target of Thalidomide: A Breakthrough for Progress in the Development of Protein Degraders. *Chem. Soc. Rev.* **2022**, *51* (15), 6234–6250.

(10) Ito, T.; Ando, H.; Suzuki, T.; Ogura, T.; Hotta, K.; Imamura, Y.; Yamaguchi, Y.; Handa, H. Identification of a Primary Target of Thalidomide Teratogenicity. *Science* **2010**, *327* (5971), 1345–1350.

(11) Belkina, A. C.; Denis, G. V. BET Domain Co-Regulators in Obesity, Inflammation and Cancer. *Nat. Rev. Cancer* **2012**, *12* (7), 465–477.

(12) Roy, M. J.; Winkler, S.; Hughes, S. J.; Whitworth, C.; Galant, M.; Farnaby, W.; Rumpel, K.; Ciulli, A. SPR-Measured Dissociation Kinetics of PROTAC Ternary Complexes Influence Target Degradation Rate. *ACS Chem. Biol.* **2019**, *14* (3), 361–368.

(13) Riching, K. M.; Mahan, S.; Corona, C. R.; McDougall, M.; Vasta, J. D.; Robers, M. B.; Urh, M.; Daniels, D. L. Quantitative Live-Cell Kinetic Degradation and Mechanistic Profiling of PROTAC Mode of Action. *ACS Chem. Biol.* **2018**, *13* (9), 2758–2770.

(14) Dragovich, P. S.; Pillow, T. H.; Blake, R. A.; Sadowsky, J. D.; Adaligil, E.; Adhikari, P.; Chen, J.; Corr, N.; Dela Cruz-Chuh, J.; Del Rosario, G.; Fullerton, A.; Hartman, S. J.; Jiang, F.; Kaufman, S.; Kleinheinz, T.; Kozak, K. R.; Liu, L.; Lu, Y.; Mulvihill, M. M.; Murray, J. M.; O'Donohue, A.; Rowntree, R. K.; Sawyer, W. S.; Staben, L. R.; Wai, J.; Wang, J.; Wei, B.; Wei, W.; Xu, Z.; Yao, H.; Yu, S.-F.; Zhang, D.; Zhang, H.; Zhang, S.; Zhao, Y.; Zhou, H.; Zhu, X. Antibody-Mediated Delivery of Chimeric BRD4 Degraders. Part 2: Improvement of In Vitro Antiproliferation Activity and In Vivo Antitumor Efficacy. *J. Med. Chem.* **2021**, *64* (5), 2576–2607.

(15) Riching, K. M.; Vasta, J. D.; Hughes, S. J.; Zoppi, V.; Maniaci, C.; Testa, A.; Urh, M.; Ciulli, A.; Daniels, D. L. Translating PROTAC Chemical Series Optimization into Functional Outcomes Underlying BRD7 and BRD9 Protein Degradation. *Curr. Res. Chem. Biol.* **2021**, *1*, No. 100009.

(16) Bondeson, D. P.; Smith, B. E.; Burslem, G. M.; Buhimschi, A. D.; Hines, J.; Jaime-Figueroa, S.; Wang, J.; Hamman, B. D.; Ishchenko, A.; Crews, C. M. Lessons in PROTAC Design from Selective Degradation with a Promiscuous Warhead. *Cell Chem. Biol.* **2018**, *25* (1), 78–87.e5.

(17) Mak, S.; Marszal, A.; Matscheko, N.; Rant, U. Kinetic Analysis of Ternary and Binary Binding Modes of the Bispecific Antibody Emicizumab. *mAbs* **2023**, *15* (1), No. 2149053.

(18) Daub, H.; Traxler, L.; Ismajli, F.; Groitl, B.; Itzen, A.; Rant, U. The Trimer to Monomer Transition of Tumor Necrosis Factor-Alpha Is a Dynamic Process That Is Significantly Altered by Therapeutic Antibodies. *Sci. Rep.* **2020**, *10* (1), 9265.

(19) Kast, F.; Schwill, M.; Stüber, J. C.; Pfundstein, S.; Nagy-Davidescu, G.; Rodríguez, J. M. M.; Seehusen, F.; Richter, C. P.; Honegger, A.; Hartmann, K. P.; Weber, T. G.; Kroener, F.; Ernst, P.; Piehler, J.; Plückthun, A. Engineering an Anti-HER2 Biparatopic Antibody with a Multimodal Mechanism of Action. *Nat. Commun.* **2021**, *12* (1), 3790.

(20) Nemoz, C.; Ropars, V.; Frit, P.; Gontier, A.; Drevet, P.; Yu, J.; Guerois, R.; Pitois, A.; Comte, A.; Delteil, C.; Barboule, N.; Legrand, P.; Baconnais, S.; Yin, Y.; Tadi, S.; Barbet-Massin, E.; Berger, I.; Le Cam, E.; Modesti, M.; Rothenberg, E.; Calsou, P.; Charbonnier, J. B. XLF and APLF Bind Ku80 at Two Remote Sites to Ensure DNA Repair by Non-Homologous End Joining. *Nat. Struct. Mol. Biol.* **2018**, *25* (10), 971–980.

(21) Sijacki, T.; Alcón, P.; Chen, Z. A.; McLaughlin, S. H.; Shakeel, S.; Rappsilber, J.; Passmore, L. A. The DNA-Damage Kinase ATR Activates the FANCD2-FANCI Clamp by Priming It for Ubiquitination. *Nat. Struct. Mol. Biol.* **2022**, *29* (9), 881–890.

(22) Higuera-Rodriguez, R. A.; Pascali, M. C. D.; Aziz, M.; Sattler, M.; Rant, U.; Kaiser, W. Kinetic FRET Assay to Measure Binding-Induced Conformational Changes of Nucleic Acids. *ACS Sens.* **2023**, *8*, 4597.

(23) Snodin, B. E. K.; Randisi, F.; Mosayebi, M.; Šulc, P.; Schreck, J. S.; Romano, F.; Ouldridge, T. E.; Tsukanov, R.; Nir, E.; Louis, A. A.; Doye, J. P. K. Introducing Improved Structural Properties and Salt Dependence into a Coarse-Grained Model of DNA. *J. Chem. Phys.* **2015**, *142* (23), No. 234901.

https://doi.org/10.1021/acssensors.5c04944
ACS Sens. XXXX, XXX, XXX−XXX

(24) Gadd, M. S.; Testa, A.; Lucas, X.; Chan, K.-H.; Chen, W.; Lamont, D. J.; Zengerle, M.; Ciulli, A. Structural Basis of PROTAC Cooperative Recognition for Selective Protein Degradation. *Nat. Chem. Biol.* **2017**, *13* (5), 514–521.
(25) Stennett, E. M. S.; Ciuba, M. A.; Levitus, M. Photophysical Processes in Single Molecule Organic Fluorescent Probes. *Chem. Soc. Rev.* **2014**, *43* (4), 1057–1075.
(26) Navratilova, I.; Aristotelous, T.; Picaud, S.; Chaikuad, A.; Knapp, S.; Filappakopoulos, P.; Hopkins, A. L. Discovery of New Bromodomain Scaffolds by Biosensor Fragment Screening. *ACS Med. Chem. Lett.* **2016**, *7* (12), 1213–1218.
(27) Philpott, M.; Yang, J.; Tumber, T.; Fedorov, O.; Uttarkar, S.; Filippakopoulos, P.; Picaud, S.; Keates, T.; Felletar, I.; Ciulli, A.; Knapp, S.; Heightman, T. D. Bromodomain-Peptide Displacement Assays for Interactome Mapping and Inhibitor Discovery. *Mol. Biosyst.* **2011**, *7* (10), 2899–2908.
(28) Deinum, J.; Gustavsson, L.; Gyzander, E.; Kullman-Magnusson, M.; Edström, A.; Karlsson, R. A Thermodynamic Characterization of the Binding of Thrombin Inhibitors to Human Thrombin, Combining Biosensor Technology, Stopped-Flow Spectrophotometry, and Microcalorimetry. *Anal. Biochem.* **2002**, *300* (2), 152–162.
(29) Douglass, E. F.; Miller, C. J.; Sparer, G.; Shapiro, H.; Spiegel, D. A. A Comprehensive Mathematical Model for Three-Body Binding Equilibria. *J. Am. Chem. Soc.* **2013**, *135* (16), 6092–6099.
(30) Winter, G. E.; Mayer, A.; Buckley, D. L.; Erb, M. A.; Roderick, J. E.; Vittori, S.; Reyes, J. M.; Di Iulio, J.; Souza, A.; Ott, C. J.; Roberts, J. M.; Zeid, R.; Scott, T. G.; Paulk, J.; Lachance, K.; Olson, C. M.; Dastjerdi, S.; Bauer, S.; Lin, C. Y.; Gray, N. S.; Kelliher, M. A.; Churchman, L. S.; Bradner, J. E. BET Bromodomain Proteins Function as Master Transcription Elongation Factors Independent of CDK9 Recruitment. *Mol. Cell* **2017**, *67* (1), 5–18.e19.
(31) Werner, M. T.; Wang, H.; Hamagami, N.; Hsu, S. C.; Yano, J. A.; Stonestrom, A. J.; Behera, V.; Zong, Y.; Mackay, J. P.; Blobel, G. A. Comparative Structure-Function Analysis of Bromodomain and Extraterminal Motif (BET) Proteins in a Gene-Complementation System. *J. Biol. Chem.* **2020**, *295* (7), 1898–1914.
(32) Filippakopoulos, P.; Qi, J.; Picaud, S.; Shen, Y.; Smith, W. B.; Fedorov, O.; Morse, E. M.; Keates, T.; Hickman, T. T.; Felletar, I.; Philpott, M.; Munro, S.; McKeown, M. R.; Wang, Y.; Christie, A. L.; West, N.; Cameron, M. J.; Schwartz, B.; Heightman, T. D.; La Thangue, N.; French, C. A.; Wiest, O.; Kung, A. L.; Knapp, S.; Bradner, J. E. Selective Inhibition of BET Bromodomains. *Nature* **2010**, *468* (7327), 1067–1073.
(33) Nicodeme, E.; Jeffrey, K. L.; Schaefer, U.; Beinke, S.; Dewell, S.; Chung, C.; Chandwani, R.; Marazzi, I.; Wilson, P.; Coste, H.; White, J.; Kirilovsky, J.; Rice, C. M.; Lora, J. M.; Prinjha, R. K.; Lee, K.; Tarakhovsky, A. Suppression of Inflammation by a Synthetic Histone Mimic. *Nature* **2010**, *468* (7327), 1119–1123.
(34) Anders, L.; Guenther, M. G.; Qi, J.; Fan, Z. P.; Marineau, J. J.; Rahl, P. B.; Lovén, J.; Sigova, A. A.; Smith, W. B.; Lee, T. I.; Bradner, J. E.; Young, R. A. Genome-Wide Localization of Small Molecules. *Nat. Biotechnol.* **2014**, *32* (1), 92–96.
(35) Pan, Z.; Zhao, Y.; Wang, X.; Xie, X.; Liu, M.; Zhang, K.; Wang, L.; Bai, D.; Foster, L. J.; Shu, R.; He, G. Targeting Bromodomain-Containing Proteins: Research Advances of Drug Discovery. *Mol. Biomed.* **2023**, *4* (1), 13.
(36) Nowak, R. P.; DeAngelo, S. L.; Buckley, D.; He, Z.; Donovan, K. A.; An, J.; Safaee, N.; Jedrychowski, M. P.; Ponthier, C. M.; Ishoey, M.; Zhang, T.; Mancias, J. D.; Gray, N. S.; Bradner, J. E.; Fischer, E. S. Plasticity in Binding Confers Selectivity in Ligand-Induced Protein Degradation. *Nat. Chem. Biol.* **2018**, *14* (7), 706–714.
(37) Zengerle, M.; Chan, K.-H.; Ciulli, A. Selective Small Molecule Induced Degradation of the BET Bromodomain Protein BRD4. *ACS Chem. Biol.* **2015**, *10* (8), 1770–1777.
(38) Hsia, O.; Hinterndorfer, M.; Cowan, A. D.; Iso, K.; Ishida, T.; Sundaramoorthy, R.; Nakasone, M. A.; Imrichova, H.; Schätz, C.; Rukavina, A.; Husnjak, K.; Wegner, M.; Correa-Sáez, A.; Craigon, C.; Casement, R.; Maniaci, C.; Testa, A.; Kaulich, M.; Dikic, I.; Winter, G. E.; Ciulli, A. Targeted Protein Degradation via Intramolecular Bivalent Glues. *Nature* **2024**, *627*, 204.
(39) Ichikawa, S.; Payne, N. C.; Xu, W.; Chang, C.-F.; Vallavoju, N.; Frome, S.; Flaxman, H. A.; Mazitschek, R.; Woo, C. M. The Cyclimids: Degron-Inspired Cereblon Binders for Targeted Protein Degradation. *Cell Chem. Biol.* **2024**, *31*, 1162.
(40) Wurz, R. P.; Rui, H.; Dellamaggiore, K.; Ghimire-Rijal, S.; Choi, K.; Smither, K.; Amegadzie, A.; Chen, N.; Li, X.; Banerjee, A.; Chen, Q.; Mohl, D.; Vaish, A. Affinity and Cooperativity Modulate Ternary Complex Formation to Drive Targeted Protein Degradation. *Nat. Commun.* **2023**, *14* (1), 4177.
(41) Bauer, K.; Berghoff, A. S.; Preusser, M.; Heller, G.; Zielinski, C. C.; Valent, P.; Grunt, T. W. Degradation of BRD4—a Promising Treatment Approach Not Only for Hematologic but Also for Solid Cancer. *Am. J. Cancer Res.* **2021**, *11* (2), 530–545.
(42) Nowak, R. P.; Yue, H.; Park, E. Y.; Fischer, E. S. *Methods for Quantitative Assessment of Protein Degradation*. In Targeted Protein Degradation; Cacace, A. M., Hickey, C. M., Békés, M., Eds.; Methods in Molecular Biology; Springer US: New York, NY, **2021**; Vol. 2365, pp 247−263.
(43) Kim, S. A.; Go, A.; Jo, S.-H.; Park, S. J.; Jeon, Y. U.; Kim, J. E.; Lee, H. K.; Park, C. H.; Lee, C.-O.; Park, S. G.; Kim, P.; Park, B. C.; Cho, S. Y.; Kim, S.; Ha, J. D.; Kim, J.-H.; Hwang, J. Y. A Novel Cereblon Modulator for Targeted Protein Degradation. *Eur. J. Med. Chem.* **2019**, *166*, 65–74.
(44) Edmondson, S. D.; Yang, B.; Fallan, C. Proteolysis Targeting Chimeras (PROTACs) in "beyond Rule-of-Five" Chemical Space: Recent Progress and Future Challenges. *Bioorg. Med. Chem. Lett.* **2019**, *29* (13), 1555–1564.
(45) Wu, S.; Jiang, Y.; Hong, Y.; Chu, X.; Zhang, Z.; Tao, Y.; Fan, Z.; Bai, Z.; Li, X.; Chen, Y.; Li, Z.; Ding, X.; Lv, H.; Du, X.; Lim, S. L.; Zhang, Y.; Huang, S.; Lu, J.; Pan, J.; Hu, S. BRD4 PROTAC Degrader ARV-825 Inhibits T-Cell Acute Lymphoblastic Leukemia by Targeting "Undruggable" Myc-Pathway Genes. *Cancer Cell Int.* **2021**, *21* (1), 230.
(46) Zhu, X.; Liu, W.; Tang, X.; Chen, Y.; Ge, X.; Ke, Q.; Liang, X.; Gan, Y.; Zheng, Y.; Zou, M.; Deng, M.; Liu, Y.; Li, D. W.-C.; Gong, L. The BET PROTAC Inhibitor dBET6 Protects against Retinal Degeneration and Inhibits the cGAS-STING in Response to Light Damage. *J. Neuroinflammation* **2023**, *20* (1), 119.
(47) Xu, L.; Chen, Y.; Mayakonda, A.; Koh, L.; Chong, Y. K.; Buckley, D. L.; Sandanaraj, E.; Lim, S. W.; Lin, R. Y.-T.; Ke, X.-Y.; Huang, M.-L.; Chen, J.; Sun, W.; Wang, L.-Z.; Goh, B. C.; Dinh, H. Q.; Kappei, D.; Winter, G. E.; Ding, L.-W.; Ang, B. T.; Berman, B. P.; Bradner, J. E.; Tang, C.; Koeffler, H. P. Targetable BET Proteins- and E2F1-Dependent Transcriptional Program Maintains the Malignancy of Glioblastoma. *Proc. Natl. Acad. Sci.* **2018**, *115* (22), E5086–E5095.
(48) Chan, K.-H.; Zengerle, M.; Testa, A.; Ciulli, A. Impact of Target Warhead and Linkage Vector on Inducing Protein Degradation: Comparison of Bromodomain and Extra-Terminal (BET) Degraders Derived from Triazolodiazepine (JQ1) and Tetrahydroquinoline (I-BET726) BET Inhibitor Scaffolds. *J. Med. Chem.* **2018**, *61* (2), 504–513.
(49) Liu, X.; Ciulli, A. Proximity-Based Modalities for Biology and Medicine. *ACS Cent. Sci.* **2023**, *9* (7), 1269–1284.
(50) Cao, S.; Kang, S.; Mao, H.; Yao, J.; Gu, L.; Zheng, N. Defining Molecular Glues with a Dual-Nanobody Cannabidiol Sensor. *Nat. Commun.* **2022**, *13* (1), 815.
(51) Raina, K.; Forbes, C.D.; Stronk, R.; Rappi, J.P.; Eastman, K.J.; Zaware, N.; Yu, X.; Li, H.; Bhardwaj, A.; Gerritz, S.W.; Forgione, M.; Hundt, A.; King, M.P.; Posner, Z.M.; Correia, A.D.; McGovern, A.; Puleo, D.E.; Chenard, R.; Mousseau, J.J.; Vergara, J.I.; Garvin, E.; Macaluso, J.; Martin, M.; Bassoli, K.; Jones, K.; Garcia, M.; Howard, K.; Yaggi, M.; Smith, L.M.; Chen, J.M.; Mayfield, A.B.; De Leon, C.A.; Hines, J.; Kayser-Bricker, K.J.; Crews, C.M. Regulated induced proximity targeting chimeras-RIPTACs-A heterobifunctional small

https://doi.org/10.1021/acssensors.5c04944
ACS Sens. XXXX, XXX, XXX−XXX

molecule strategy for cancer selective therapies. *Cell. Chem. Biol.* **2024**, *31* (8), 1490–1502.e42.
(52) Gourisankar, S.; Krokhotin, A.; Ji, W.; Liu, X.; Chang, C.-Y.; Kim, S. H.; Li, Z.; Wenderski, W.; Simanauskaite, J. M.; Yang, H.; Vogel, H.; Zhang, T.; Green, M. R.; Gray, N. S.; Crabtree, G. R. Rewiring Cancer Drivers to Activate Apoptosis. *Nature* **2023**, *620* (7973), 417–425.

https://doi.org/10.1021/acssensors.5c04944
ACS Sens. XXXX, XXX, XXX–XXX